International Journal of Environmental Sciences
ISSN: 2229-7359
Vol. 12 No. 1, 2026
https://theaspd.com/index.php

Photocatalytic Activity of Natao$_3$ Nanoparticles Synthesized by Facile Hydrothermal Method for the Degradation of Diazo Evans Blue Dye

Hina Anjum Kouser [a], H. S. Bhojya Naik [a*], G. P. Mamatha[b], K. M. Pallavi[b], S. Pampapathi[b], E. Vinay Kumar[c], G. Nagaraju[d*]

[a]Department of Studies and Research in Industrial Chemistry School of Chemical Sciences, Kuvempu University, Shankaragatta 577451, India

[b] Department of Studies in Chemistry, Davangere University, Shivagangothri, Davangere 577 007 Karnataka, India.

[c]Department of Studies and Research in Industrial Chemistry, Sahyadri Science College, Kuvempu University, Shivamogga 577 203, India

[d] Energy Materials Research Laboratory, Department of Chemistry, Siddaganga Institute of Technology, Tumakuru, Karnataka 572 103, India

Abstract

In this study, $NaTaO_3$ nanoparticles (NPs) were synthesized by a simple one step hydrothermal method. XRD, FTIR, FESEM, EDS, TEM, elemental mapping, UV-Vis, and PL spectroscopy were used to assess the structural clarity, particle size, shape, porosity features, and optical properties of the $NaTaO_3$ NPs. The findings indicated that pure-phase $NaTaO_3$ could be synthesized using 10 M NaOH solution at 150 ^{0}C for 24 h. $NaTaO_3$ NPs exhibits significant photodegradation activity for Evans blue dye. The photocatalyst have been optimized for multiple photocatalytic degradation factors, such as pH, catalyst load effect, and dye starting concentration variation. The synthesised photocatalyst shows 97% degradation capacity for Evans blue dye. According to the study, the catalyst is photostable because it is used for nearly four cycles and it shows satisfactory dye degradation efficiency.

Keywords: *Perovskite, Hydrothermal synthesis, $NaTaO_3$ NPs, Dye degradation.*

1. INTRODUCTION

The textile, cosmetics, and pharmaceutical industries release dyes, which are classified as toxic compounds due to their long-term persistence and detrimental effects [1-3]. To eliminate contaminants, numerous physical, biological, and Chemical technologies have been used. [4-6]. Bioremediation methods, such as fungal biodegradation [7], bacterial biodegradation [8], and biosorption [9], are environmentally friendly and protective of the environment during the treatment process. In contrast, organic pollution treatment procedures, such as oxidation, reduction, or adsorption, are complex, costly, and ineffective [10-15]. It has been demonstrated that adsorption and other traditional physical techniques are successful in eliminating organic dyes. However, they necessitate an additional and time-consuming process to regenerate the exhausted adsorbents after adsorption.

Because of its high effectiveness, the elimination of colors from wastewater using light exposure combined with a catalyst has garnered significant attention. One of the most popular technique utilized for the treatment of trash is photocatalytic degradation (PCD) using sustainable UV/visible light due to its effectiveness, simplicity of operation, and low-cost metal oxide photocatalysts exhibit remarkable potential in the processing of wastewater under UV/visible light due to their exceptional characteristics [16-20]. These include low toxicity, stability, ease of synthesis, suitable bandgap, and efficient formation of active oxygen species. Consequently, photocatalysis applications utilizing visible and UV radiation have received the majority of attention [21-23].

Metal oxide semiconductor-based photocatalysis is the gold standard for removing pollutants from the environment. Ozone semiconductor NPs are gaining attention due to their intriguing functional properties linked to their high active surface and small particle size [24]. This is due to the fact that these NPs are applicable to a wide range of industries, such as sensing and wastewater treatment [25, 26]. Heterogeneous

photocatalysts, in particular ZnS, ZnO, CdS, GaP, CdO, and TiO_2, are widely used due to their full mineralization and superior pollutant degradation [27-32]. These photocatalysts possess a number of significant benefits, including the capability of being affordable, stable, aggressively oxidizing, and nontoxic [33-35]. Among the many applications for these heterogeneous photocatalysts are antibacterial activity, organic and dye degradation, CO_2 reduction, and hydrogen production [36-40].

NaTa oxide, also known as $NaTaO_3$, is a novel form of A semiconductor made of perovskite oxide that has garnered a lot of interest in photocatalysis applications, including water splitting, hydrogen evolution, and organic pollutant photodegradation [41,42]. As stated by the Jiang group, in the presence of ultraviolet (UV) light, the pyrochlore-like $Na_2Ta_2O_6$ nanocubes with a broad bandgap (~4.6 eV) demonstrated exceptional photocatalytic properties. Li group used the hydrothermal approach to create a NaTa trioxide ($NaTaO_3$) nanocube of the perovskite-type. They discovered that the perovskite-type $NaTaO_3$ (NT) nanocubes have a better capacity for H_2 evolution under UV light and an extrapolating bandgap (about 4.6 eV) than the pyrochlore-like $Na_2Ta_2O_6$ nanocubes. The increased activity suggested that the perovskite-type NT is a catalyst that shows a lot of potential for photocatalysis. Consequently, increasing NT's photocatalytic activity is crucial. One key component of the photocatalytic property is the morphology of the photocatalyst. For instance, several morphologies of $Na_2Ta_2O_6$ nanocrystalline, which were created by varying the proportion of NaOH, demonstrated a noticeable variation in photocatalytic activity. The NT's photocatalytic activity can be enhanced by modifying its shape. According to certain papers, Excellent photocatalytic activity was shown using tubular nano photocatalysts in contrast to nanowires and nanocubes, among other morphologies. NT NPs have been synthesised in multiple methodologies like solvothermal [43], hydrothermal [44], solid-state chemical reaction [45], chemical precipitation [46], sol-gel method [47,48], etc.

The objective of this research project is to develop long-lasting techniques for treatment of water, which is crucial to preserve water supplies and ensure the welfare of future generations, and develop more effective, economical, and ecologically friendly photocatalysts utilizing a hydrothermal approach.

2. Experimental

2.1. Chemicals and devices

Only analytical-grade chemicals were used in each step of the study. Sodium hydroxide was collected from HI media laboratories (Mumbai, India) with the highest available purity. We purchased tantalum (V) chloride from Sigma Ltd. in Bangalore, India.

With the aid of a Rigaku Smart lab X-ray diffractometer (XRD) with Cu-Kα (1.5418 Å) radiation with a nickel filter, The purity of the phase and crystallinity of synthesized NPs are examined. Metal oxide Analysis of bonding interactions was done using the Bruker-Alpha FT-IR spectrophotometer from the KBr pellet method. Utilizing a LAB INDIA UV 3092 spectrophotometer, the optical characteristics were assessed. The surface morphology of the The produced NPs were examined using (FESEM- CARLZEISS Ultra 55) Scanning electron microscope, and high-resolution transmission electron microscopy (HR-TEM) was utilized to describe the nanoparticle's size, shape, and internal structures. "HEBER" scientific UV–Visible annular photoreactor were employed to perform PCD of Evans blue (EB) using perovskite NT NPs.

2.2. Synthesis of NT NPs

Compared to the traditional high-temperature reaction, the hydrothermal approach is the cost effective, energy-saving, and simple method to synthesize crystalline NT with nano size. 0.2 g $TaCl_5$ powder dissolved in 10 mL ethanol and this solution was mixed in 10 M NaOH. and stirred on a magnetic stirrer at room temperature (RT) for about 60 min, then obtained white-colored The solution was put in into a Teflon-lined autoclave (capacity 100 mL) and heated at 150^0C for 24 hours. The white precipitate that produced was dried for 12 hours at 80°C following two distilled water washes and then ethanol.

3. RESULTS AND DISCUSSION

3.1. XRD analysis (Crystal structure)

The XRD pattern of the obtained pure perovskite NT NPs is depicted in Fig. 1. Every diffraction peak are attributed to a pure monoclinic phase of crystalline NT. There are nine obvious diffraction peaks in this

pattern. The diffraction peaks (1 0 0), (1 1 0), (-1 1 1), (2 0 0), (2 1 0), (-211), (220) (-221), (310) and (-311) at different d-spacing can be indexed as pure perovskite structure (NT) according to the standard card (JCPDS-ICDD card No. 74-2480), which demonstrated that NT was the only phase formed during the process. The greater crystalline character of NT is revealed by the sharp XRD peak. By using XRD data, By applying the Debye Scherrer equation, the crystallite size of NT samples was calculated.

$D = K\lambda/\beta \cos\theta$

Where D is crystallite size, λ is X-ray wavelength (1.54 A°), β is full-width half maxima, and K is Scherrer constant (0.94). The calculated average crystallite size of NT NPs were found to be in the range of 71 nm

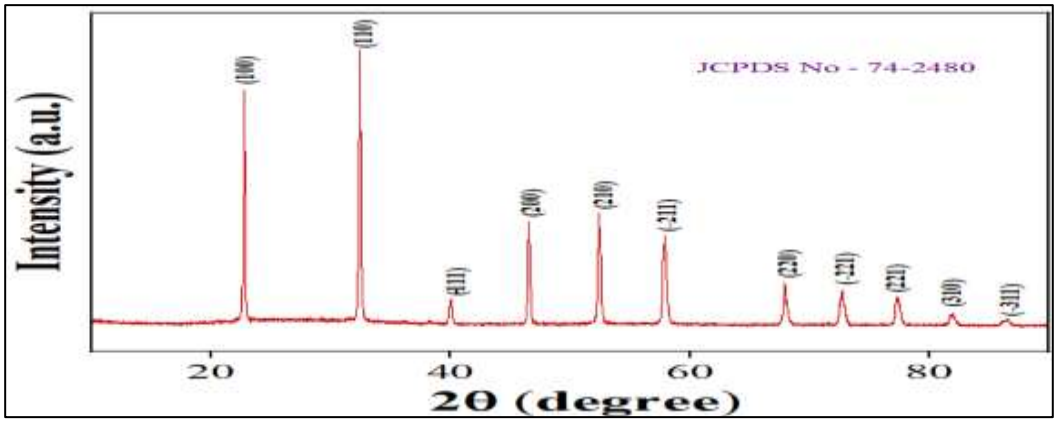

Fig. 1. XRD patterns of the as-prepared NT NPs.

3.2. FT-IR analysis

The chemical functionalization of nanocrystalline NT samples was investigated using FT-IR analysis as depicted in Fig. 2. The fingerprint peak responsible for Ta—O vibrations was observed at 642 cm^{-1}. The Ta—O stretching and Ta—O—Ta bridge stretching modes are responsible for the Ta—O band in the spectrum.[50]. The band at 1585 and 3424 cm^{-1} are because of the bending and stretching vibration of water molecules that have been adsorbed onto NT NPs surface.

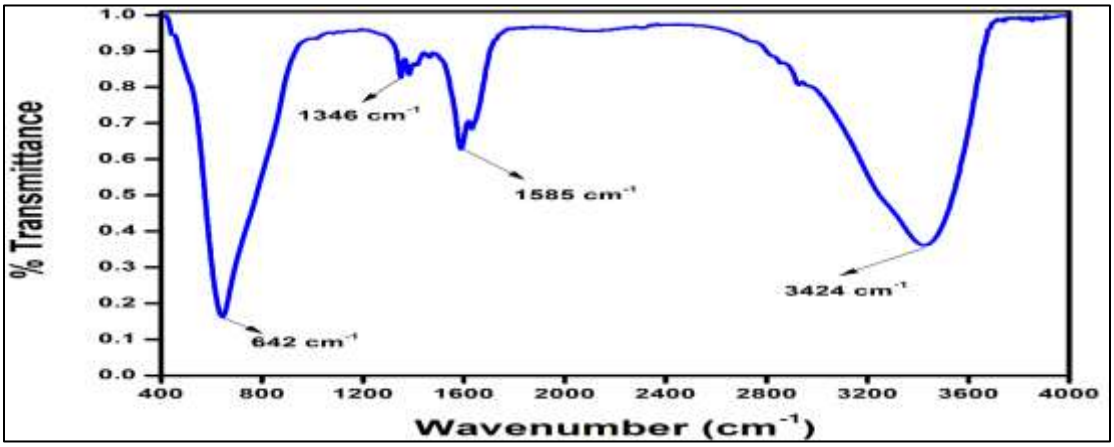

Fig. 2. FT-IR spectrum of as-prepared NT NPs.

3.3. UV–Vis analysis

The NT NPs' photo absorbance was examined using a UV-vis spectrometer. Fig. 3a shows the typical absorbance spectra of NT, the absorption peak present in the wavelength between 300 to 380 nm, shows that the NT was capable of absorbing strong UV radiation with high absorbance implying the material is capably employed as an organic UV blocker rather than organic absorber. This band arises because of electrons

moving from the valence band (VB) to the conduction band (CB). The following equation was applied to ascertain the energy bandgap of the synthesized NT NPs [50].

$\alpha = A (h\upsilon - E_g)^{n/2}/h\upsilon$ .....(2)

where α, υ, Eg, and n stand for the absorption coefficient, absorption frequency, band gap, constant, and integer, respectively. The calculated energy band gap (E_g) of the NT NPs found to be 3.05 eV as depicted in Fig. 3b obtained by plotting energy (eV) of photons versus $(\alpha h\nu)^2$

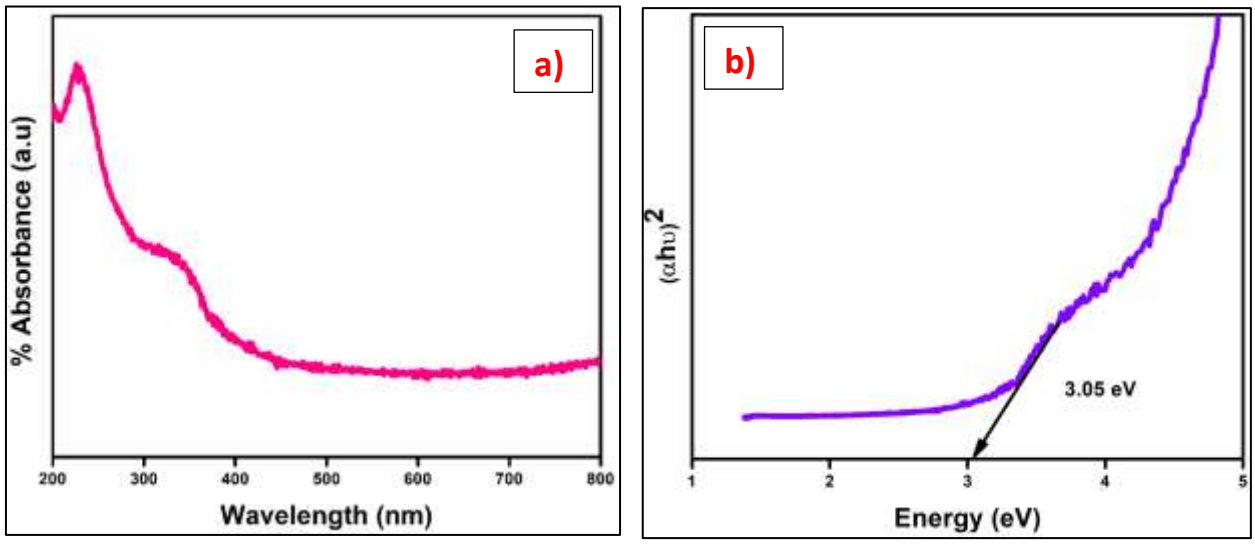

Fig. 3. a) UV-Vis absorbance spectrum, and **b)** plot of $(\alpha h\nu)^2$ versus Energy showing the energy bandgap of NT NPs.

3.4. SEM and EDAX studies

Figure 4(a, b) demonstrates the SEM images of NT NPs exhibit cubic morphology. As known, NT is an ABO_3 perovskite-type structure, where TaO_6 tetrahedra are coupled in a corner-sharing arrangement, allowing the establishment of cubic morphology [51]. The elemental composition of the as-prepared NT was estimated by the EDS aspect given in Fig. 4d. which displays the EDS spectrum derived for NT NPs, indicating the presence and consistency of O, Na, and Ta with atomic percentages (showed in the inset Fig. 4d). The uniform distribution of the elements in the prepared NT sample was confirmed by the elemental mapping with colors red, green, and, blue for the elements O, Na, and Ta respectively, as outlined in Fig. 5(a-c).

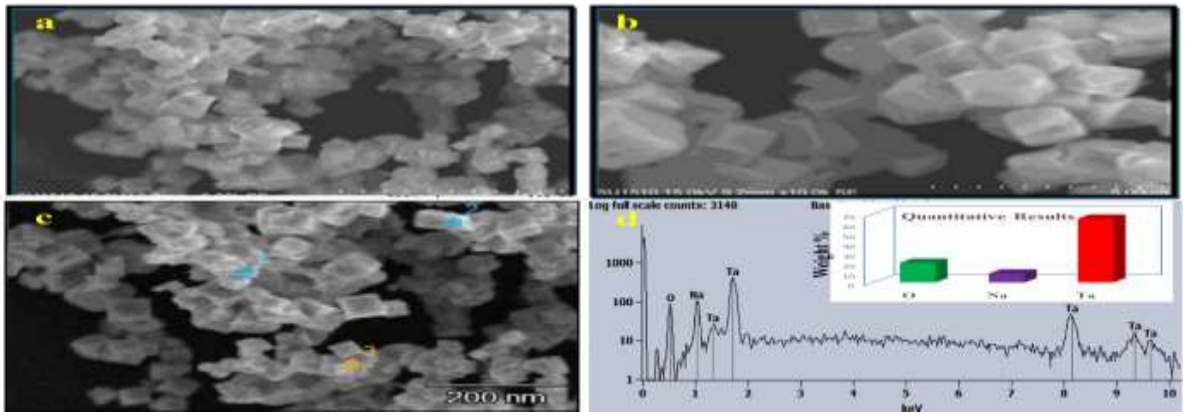

Fig. 4. FE-SEM images (**a** and **c**). low-magnification and (**b**) high-magnification SEM images. and **d.** EDS spectrum of the as-prepared NT NPs with composition.

International Journal of Environmental Sciences
ISSN: 2229-7359
Vol. 12 No. 1, 2026
https://theaspd.com/index.php

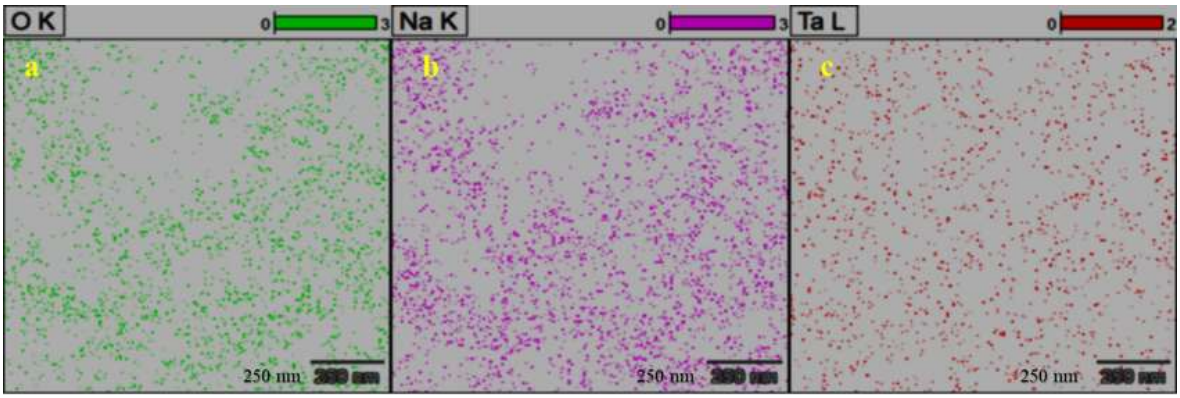

Fig. 5. a-c. Elemental mapping of NT NPs. Elemental mapping of **a.** oxygen, **b.** sodium, and **c.** Tantalum.

3.5. TEM analysis

Using TEM analysis, more structural characterisation was carried out. The existence of nanocubes is revealed by the TEM image of NT NPs in Fig. 6(a, b). The synthesised NT nanocubes' crystallinity is confirmed by the selected area electron diffraction (SAED) pattern. Fig. 6c displays the NTO NPs' HRTEM image. The measured d spacing of about 0.22 nm corresponds to the (-1 1 1) planes of monoclinic phase NT NPs and Fig. 6d, also with bright circular fringes in SAED pattern closely matches the d-spacing values determined by XRD information having the highest intensity planes at (1 0 0), (-1 1 0) and (2 1 0) [52].

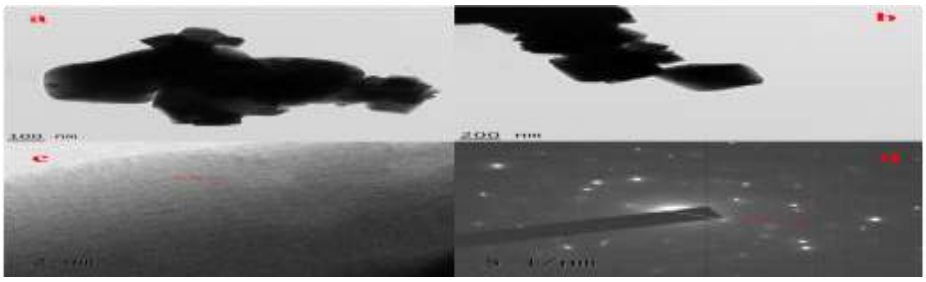

Fig. 6. a.**b**. TEM image of the NT nanocube sample. **c**. HRTEM image of a NT nanocube showing clear lattice fringes. **d.** SAED pattern of a NT nanocube.

4. Photocatalytic dye degradation

The process of PCD uses synthesized NT NPs to break down dye when exposed to UV light. For 180 min, photocatalytic tests were conducted on EB using quartz tubes and UV light to assess the mechanism of NT NPs Photocatalytic degradation. 10 to 50 mg of NT NPs were distributed and subjected to continuous mixing in a dark condition about 30 min. And UV light (250 W high pressure) exposure in 100 mL of EB dye solution with a defined concentration (4–20 ppm). Every 30 min interval, a defined volume (2 ml) of the dye solution was collected, and its absorbance spectrum was examined. To ascertain the level of deterioration, NT NPs are extracted from the solution mixture by centrifugation. The dye degradation percentage was determined using the following formula.

$$\% \text{ Degradation} = (A_o\text{-}A_t)/A_o \times 100$$

where A_o and At are initial and final concentration of dye solution at time t. By altering the parameters, Concentration of dye, pH, photocatalyst load, and the light exposure time, experiments were repeated.

4.1. The degradation of EB dye via photocatalysis

It was examined how effectively NT NPs worked as a photocatalyst for the PCD of EB and Rhodamine B (Rh-B) dyes. A 100 mL solution containing 5 ppm dye and 10 mg of photocatalyst was taken, and it was agitated for half an hour in the absence of light to reach the adsorption-desorption equilibrium. Subsequently, silicon

capillary tubes made silicon were inserted into quartz tubes for bubbling and to keep the particles from settling, and the tubes came into contact with light. As the trial went on, 2–3 milliliters of the test sample were taken every 30 min, and the absorbance wavelength was recorded using a UV-Vis spectrophotometer. After 180 minutes, 84% of the EB dye fades and less of the Rh-B dye disappears. This implies that NT photocatalyst can destroy anionic dyes more readily than cationic dyes. Thus, EB dye is chosen for more study. The rates of photodegradation of the dyes Rh-B and EB are depicted in Fig. 7.a.

4.2. Catalysts vary

NT NPs were added in amounts between 10 mg and 50 mg while maintaining a constant dye concentration of 5 ppm. This study examined the effects of NT NPs on EB degradation under the same conditions. Fig.7.b. demonstrates that 20 mg of photocatalyst shows maximum degradation and there is no appreciable change in degradation efficiency when the catalyst dosage is increased from 30 mg to 50 mg, and that the rate of deterioration stays essentially constant after that. The turbidity of the solution increases as the NT photocatalyst concentration exceeds 30 mg, which decreases the suspension's photoactivation potential and lessens light penetration. High catalyst concentrations could be inefficient due to aggregation and light scattering.

4.3. PPM Vary

Using varying concentrations of EB solution, the impact of dye concentration on the reaction's rate was investigated. It was noted that the rate of PCD decreased as the dye concentration increased more. This could be because more molecules of the dye were obtainable for excitation and subsequent energy transfer as the dye concentration increased. However, the dye begins to function as a filter for incident light and prevents the required light intensity from reaching the dye molecules near the semiconductor particles if the concentration of EB is increased. As a result, It was noted that the rate of PCD had decreased as depicted in Fig.7.c.

4.4. pH Vary

Fig.7.d. illustrates how pH affects Evans blue PCD. The graph demonstrates how important the dye solution's pH is to the photocatalytic process. The solution's pH can be changed by adding 0.5 M HCl and 0.5 M NaOH. In basic environments, the rate of photodegradation is higher than in acidic environments. This claim is in line with the findings that were published. We looked into how different pH values, ranging from 2 to 12, affected the rate at which dyes degradedIt is demonstrated that the rate of degradation in an acidic medium is quite good. The rate of deterioration rises from 92.20% to 100% in 90 minutes of reaction time between pH 8 and 12.

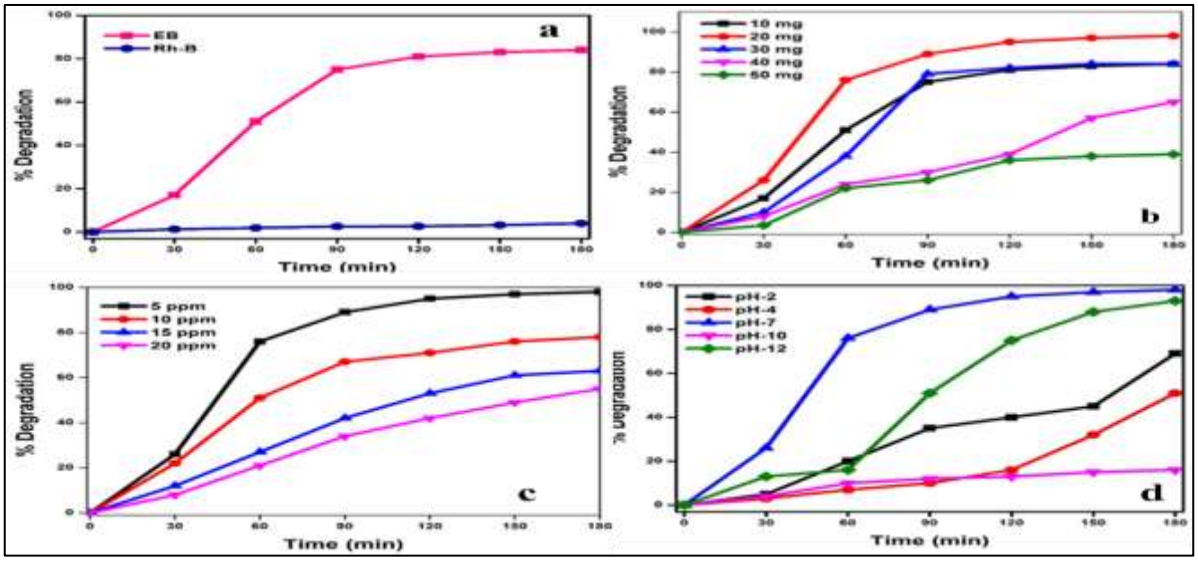

Fig. 7. PCD activity of perovskite NT NPs **a**. Catalyst optimisation **b**. Variation in catalyst dosage **c.** dye concentration **d**. varying pH.

4.5. Study of scavengers

The goal of scavenger studies on dye degradation is to understand how radical species contribute to the photocatalytic destruction of dyes. Numerous investigations on various scavengers and their impact on dye degradation mechanisms have provided information about the effectiveness and routes of these processes. Thus, $^{\bullet}O_2^-$ scavengers, $^{\bullet}OH$ radicals scavengers, h^+ scavengers, and e^- scavengers were studied using ascorbic acid (AA), tertiary butyl alcohol (TBA), EDTA, and $K_2Cr_2O_7$, respectively. Figure 8 presents the findings from EB's active species scavenger analysis. In this experiment, 5 mM quantities of AA, TBA, EDTA, and $K_2Cr_2O_7$ were added to the PCD process as $^{\bullet}O_2^-$ and h^+ scavengers. When AA was added, RB's PCD efficiency decreased noticeably in contrast to the two other radical scavengers (TBA and $K_2Cr_2O_7$). The results demonstrated that the e- and $^{\bullet}OH$ had no appreciable influence on the procedure of photodegradation. Nevertheless, in contrast to AA, the TBA scavenger's PCD of EB dye was significantly lower. Consequently, it may be claimed that upon exposure of NTA NPs to visible light, h^+, $^{\bullet}O_2^-$ and e^- Active species are necessary for the PCD of the EB dye.

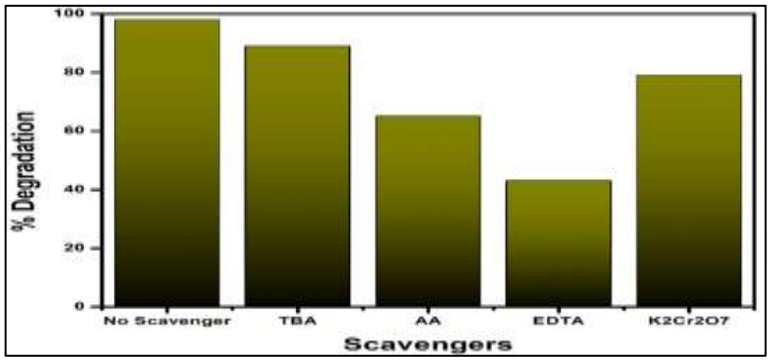

Fig. 8. Scavengers' effects on the rate of EB dye degradation.

4.6. Coumarin studies

One important factor in the photodegradation of organic dyes is the presence of hydroxyl radical ions (OH•), which are unstable and extremely active chemical entities. To ascertain whether the generated NT photocatalyst is generating the OH• radical ions, a straightforward and considerate approach of detecting OH• radical ions is to use coumarin as a substrate model. In the presence of ultraviolet light when there is a photocatalyst, 7-hydroxyl coumarin is produced from coumarin, and releases OH• free radicals. This is validated by the PL peak at 457 nm. In the present study, 20 mg of the NT photocatalyst was combined with a coumarin solution (2 mM) and subjected to UV light. After 10 minutes, 2 mL of the sample was measured using a PL device. The findings showed the production of OH• radical ions, which are required for the organic dyes' photodegradation. The NT photocatalysts' PL Spectra can be seen in Fig. 9. As the irradiation period increases, for each of the generated photocatalysts, the PL peak's strength at 456 nm rises, as seen in Figure. This implies that when irradiation time increases, •OH radical ions are continuously produced in addition to the system's enhanced production rate. Thus, the breakdown of EB occurs through a free-radical process when prepared photocatalysts are present.

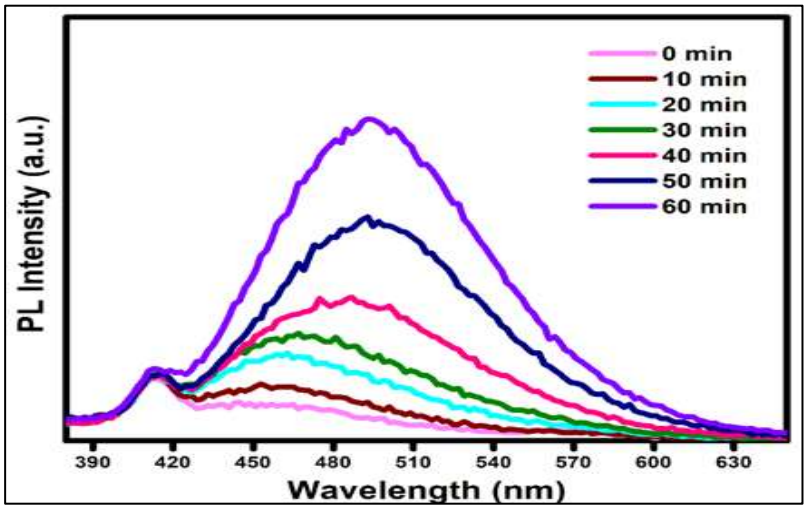

Fig. 9. Quantification of •OH radicals.

4.7. Kinetics

Fig. 10. shows the kinetic graphs of the PCD of EB dye and rhodamine-B (Rh-B) under ideal conditions. Rh-B and EB PCD reactions were carried out under ideal conditions to ascertain the order of the reaction. Plotting $\ln C_0/C$ against radiation time reveals a straight-line trend, which is observed in each scenario. The first-order rate equation

$\ln C_0/C_t = Kt$

where, C_0 (initial concentration), C_t (Final concentration), and time t, which in minutes show the substrate concentration. The slope (min-1) of the straight line can be used to determine the first-order rate constant, K. When the PCD of dyes was carried out for EB and Rh-B, respectively, the R^2 values of the experimental data was found to be 0.971 and 0.976. This confirms that dye molecule degradation follows pseudo-first-order linear kinetics.

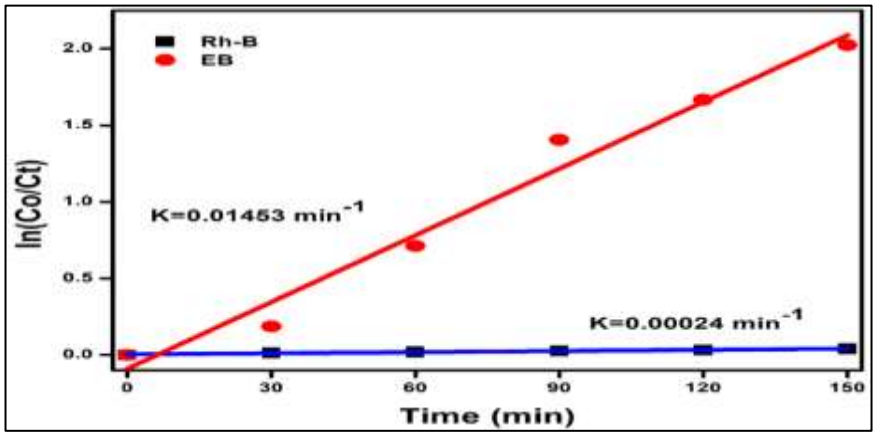

Fig. 10. Kinetics of Rh-B and EB dyes subjected to photodegradation with percentage bars

4.8. Recycling

For photocatalysts to be used in practical applications, stability is just as crucial as photocatalytic activity. By using the same NT NPs sample in the EB degradation process for five consecutive reactions, the stability of the NT NPs was also investigated. By Centrifuging the samples, nanostructured materials can be easily extracted from the solution after each step. There were marginal drops in the catalytic activity following these successful reuses of NT NPs.

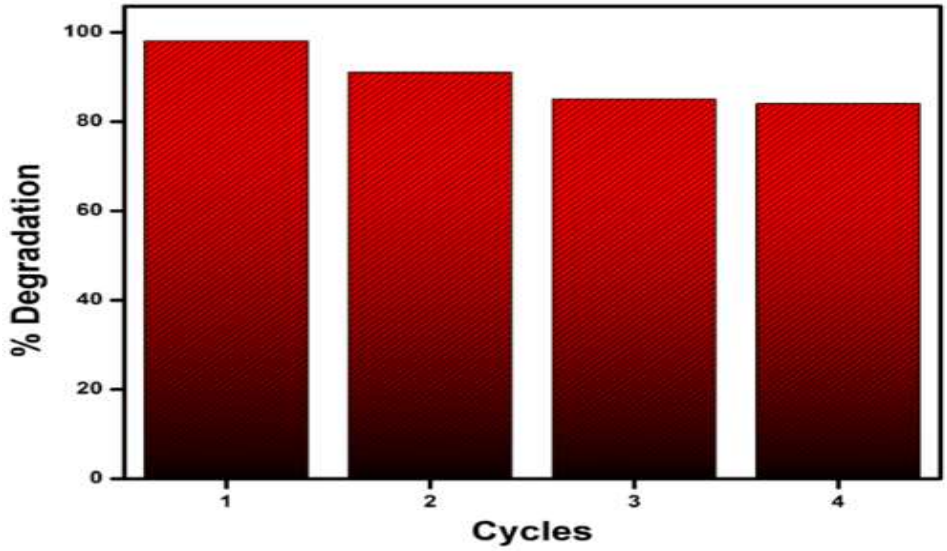

Fig. 11. Cycling experiments of photodegradation EB dye over NTO.

4.9. Degradation Mechanism

Scheme 1. explains the potential mechanism of the photo-catalytic reaction. The semiconducting NT NPs use the light energy from the incoming source to excite an electron between the conduction band (CB) and the valence band (VB) during irradiation, leaving a hole behind. Hydroxyl radicals (•OH) can be produced by this hole by abstracting electrons from water. The dyes will then be oxidized by these radicals. Additionally, $\bullet O_2^-$ active species that were generated on NTO NPs' surface may further degrade the aromatic dyes. The electronic change from VB to CB caused by light absorption and subsequent adsorption of O_2 molecules to generate $\bullet O_2^-$ active species can also be used to explain the likely mechanism. Together with the holes and photogenerated electrons, the generated $\bullet O_2^-$ also reacts to form H_2O_2, which in turn reacts with further photogenerated electrons to produce the hydroxyl radicals. Then, the dyes EB dye oxidized by both $\bullet O_2^-$ and •OH.

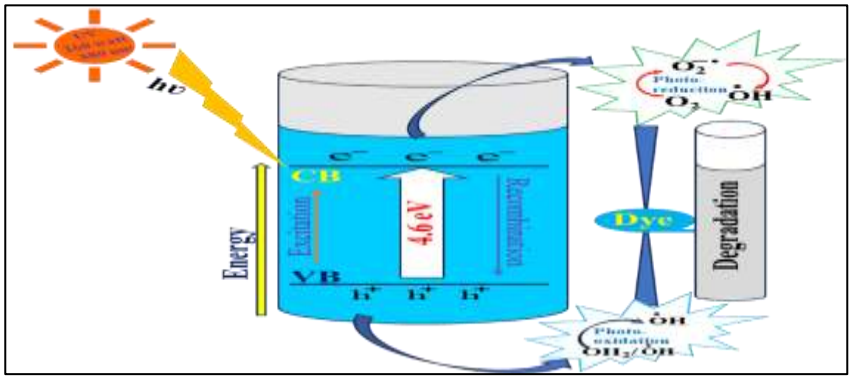

Scheme 1. Schematic mechanism for the degradation of EB.

5. CONCLUSION

Using a straightforward hydrothermal method, we developed NT nano photocatalysts. The strong XRD diffraction peaks, suggesting that the NT NPs were crystalline in nature. The produced NT NPs had cube-like shapes, according to TEM analysis. Using the Evans blue dye NT NPs' photocatalytic activity was investigated when exposed to UV light. The NT NPs showed exceptional photocatalytic activity and degraded EB at the rate of 96.2%. Additionally, the NT photocatalysts demonstrated better chemical stability. Superoxide and

hydroxyl radicals were the most common active species, according to the results of the active species trapping scavengers' studies.

ACKNOWLEDGEMENT
The authors greatly acknowledge their work to the One of the authors, Hina Anjum Kouser expresses their gratitude to the Kuvempu University. One of the authors, Dr. G. Nagaraju thanks for providing characterization techniques and the Principal, Siddaganga, Institute of Technology.

CONFLICT OF INTEREST: The authors declare no conflict of interest.

DECLARATION OF COMPETING INTEREST: The authors declare no conflict of interest.

REFERENCES

[1]. Kishor R, Purchase D, Saratale GD, Saratale RG, Ferreira LFR, Bilal M, Bharagava RN (2021) Ecotoxicological and health concerns of persistent coloring pollutants of textile industry wastewater and treatment approaches for environmental safety. J Environ Chem Eng 9(2):105012.
[2]. Bilal M, Iqbal HM (2019) An insight into toxicity and human-health-related adverse consequences of cosmeceuticals—a review. Sci Total Environ 670:555-568.
[3]. Lin J, Ye W, Xie M, Seo DH, Luo J, Wan Y, Van der Bruggen B (2023) Environmental impacts and remediation of dye-containing wastewater. Nat Rev Earth Environ 4(11): 785-803.
[4]. Ahmed SF, Mofijur M, Nuzhat S, Chowdhury AT, Rafa N, Uddin MA (2021)Show PL Recent developments in physical, biological, chemical, and hybrid treatment techniques for removing emerging contaminants from wastewater. J Hazard Mater 416:125912.
[5]. Ahmed MB, Zhou JL, Ngo HH, Guo W, Thomaidis NS, Xu J (2017) Progress in the biological and chemical treatment technologies for emerging contaminant removal from wastewater: a critical review. J Hazard Maters 323:274-298.
[6]. Saleh IA, Zouari N, Al-Ghouti MA (2020) Removal of pesticides from water and wastewater: Chemical, physical and biological treatment approaches. Environ Technol Innov 19:101026.
[7]. Dinakarkumar Y, Gnanasekaran R, Reddy, GK, Vasu V, Balamurugan P, Murali G (2024). Fungal bioremediation: An overview of the mechanisms, applications and future perspectives. J Environ Chem Ecotoxicol 6:293-302
[8] Kebede G, Tafese T, Abda EM, Kamaraj M, Assefa F (2021) Factors influencing the bacterial bioremediation of hydrocarbon contaminants in the soil: mechanisms and impacts. J Chem 2021(1):9823362.
[9]. Singh S, Kumar V, Datta S, Dhanjal DS, Sharma K, Samuel J, Singh J (2020) Current advancement and future prospect of biosorbents for bioremediation. Sci Total Environ 709:135895.
[10]. Marin ML, Santos-Juanes L, Arques A, Amat AM, Miranda, MA (2012) Organic photocatalysts for the oxidation of pollutants and model compounds. Chem. Rev 112(3):1710-1750.
[11]. Semple KT, Reid BJ, Fermor TR (2001) Impact of composting strategies on the treatment of soils contaminated with organic pollutants. Environ Pollut 112(2):269-283.
[12]. Bello MM, Raman AAA (2018) Adsorption and oxidation techniques to remove organic pollutants from water. green adsorbents for pollutant removal: fundamentals and design 249-300.
[13]. Martinez-Huitle, CA, Ferro S (2006) Electrochemical oxidation of organic pollutants for the wastewater treatment: direct and indirect processes. Chem Soc Rev 35(12):1324-1340.
[14]. Shahidi D, Roy R, Azzouz A (2015) Advances in catalytic oxidation of organic pollutants–prospects for thorough mineralization by natural clay catalysts. Appl Catal B 174:277-292.
[15]. Dong H, Zeng G, Tang L, Fan C, Zhang C, He X, He Y (2015) An overview on limitations of TiO2-based particles for photocatalytic degradation of organic pollutants and the corresponding countermeasures. Water Res 79:128-146.
[16]. Fatima B, Siddiqui SI, Rajor HK, Malik MA, Narasimharao K, Ahmad R, Kim, KH (2023) Photocatalytic removal of organic dye using green synthesized zinc oxide coupled cadmium tungstate nanocomposite under natural solar light irradiation. Environ Res 216:114534.
[17]. Al-Hakkani, MF, Gouda GA, Hassan SH, Saddik MS, El-Mokhtar MA, Ibrahim MA, Nagiub AM (2022) Cefotaxime removal enhancement via bio-nanophotocatalyst α-Fe2O3 using photocatalytic degradation technique and its echo-biomedical applications. Scientific Reports, 12(1):11881.
[18]. Weon S, He F, Choi W (2019) Status and challenges in photocatalytic nanotechnology for cleaning air polluted with volatile organic compounds: visible light utilization and catalyst deactivation. Environ Sci Nano 6(11):3185-3214.
[19]. Kumari S, Kumari A, Sharma K, Ahmed J, Jasrotia R, Kandwal A, Sharma R (2024) Enhanced Photocatalytic and Antimicrobial Performance of Divalent Metal Substituted Nickel Nanostructures for Wastewater Treatment and Biological Applications. J Inorg Organomet Polym Mater 34:5770–5790
[20]. Shah P, Unnarkat A, Patel F, Shah M, Shah PA (2022) comprehensive review on spinel based novel catalysts for visible light assisted dye degradation. Process Safety and Environmental Protection, 161:703-722.

[21]. Ahmed MA, Mohamed AA (2023) Recent progress in semiconductor/graphene photocatalysts: synthesis, photocatalytic applications, and challenges. RSC Adv 13(1):421-439.
[22]. Mohamadpour F, Amani, AM (2024) Photocatalytic systems: reactions, mechanism, and applications. RSC Adv, 14(29):20609-20645.
[23]. Ong CB, Ng LY, Mohammad AW (2018) A review of ZnO nanoparticles as solar photocatalysts: Synthesis, mechanisms and applications. Renew Sustain Energy Rev 81 :536-551.
[24]. Laurenti M, Stassi S, Canavese G, Cauda V (2017) Surface engineering of nanostructured ZnO surfaces. Adv Mater Interfaces 4(2):1600758.
[25]. Saravanan A., Kumar PS, Hemavathy RV, Jeevanantham S, Jawahar MJ, Neshaanthini J P, Saravanan R (2022) A review on synthesis methods and recent applications of nanomaterial in wastewater treatment: Challenges and future perspectives. Chemosphere, 307:135713.
[26]. Shukla S, Khan R, Daverey, A (2021) Synthesis and characterization of magnetic nanoparticles, and their applications in wastewater treatment: A review. Environmental Technology & Innovation, 24:101924.
[27]. Abdel-Azim SM, Younus MM, Dhmees A., Pannipara M, Wageh S, Galhoum AA (2022) Facile Synthesis of ZnS/1T-2H MoS2nanocomposite for Boosted adsorption/photocatalytic degradation of methylene blue under visiblelight. Environmental Science and Pollution Research, 29(57):86825-86839.
[28]. Zhang T, Wang SJ, Zhang XY, Su D, Yang Y, Wu JY, Zhao N (2019) Progress in the utilization efficiency improvement of hot carriers in plasmon-mediated heterostructure photocatalysis. Appl Sci 9(10):2093.
[29]. Jie L, Gao X, Cao X, Wu S, Long X, Ma Q, Su J (2024) A review of CdS photocatalytic nanomaterials: Morphology, synthesis methods, and applications. Materials Science in Semiconductor Processing, 176:108288.
[30]. Garcia-Segura S, Brillas E (2017) Applied photoelectrocatalysis on the degradation of organic pollutants in wastewaters, Photochem Photobiol C 31:1-35.
[31]. Warshagha MZ, Muneer M (2022) Facile synthesis of CdO-ZnO heterojunction photocatalyst for rapid removal of organic contaminants from water using visible light. Environ. Nanotechnol Monit Manag, 18:100728.
[32]. Kaplan R, Erjavec B, Dražić G, Grdadolnik J, Pintar A (2016) Simple synthesis of anatase/rutile/brookite TiO2 nanocomposite with superior mineralization potential for photocatalytic degradation of water pollutants. Appl Catal B 181:465-474.
[33]. Yadav G, Ahmaruzzaman M (2022) New generation advanced nanomaterials for photocatalytic abatement of phenolic compounds. Chemosphere, 304:135297.
[34]. Chan SHS, Yeong Wu T, Juan JC, Teh CY (2011) Recent developments of metal oxide semiconductors as photocatalysts in advanced oxidation processes (AOPs) for treatment of dye waste-water. Journal of Chemical Technology & Biotechnology, 86(9):1130-1158.
[35]. Friehs E, AlSalka Y, Jonczyk R, Lavrentieva A, Jochums A, Walter JG, Bahnemann D (2016) Toxicity, phototoxicity and biocidal activity of nanoparticles employed in photocatalysis. J Photochem Photobiol C , 29:1-28.
[36]. Yousefi SR, Alshamsi HA, Amiri O, Salavati-Niasari, M (2021) Synthesis, characterization and application of Co/Co3O4 nanocomposites as an effective photocatalyst for discoloration of organic dye contaminants in wastewater and antibacterial properties. J. Mole. Liq, 337 116405.
[37]. Tahir, MB, Asiri AM, Nawaz T (2020) A perspective on the fabrication of heterogeneous photocatalysts for enhanced hydrogen production. Int J Hydrogen Energy, 45(46):24544-24557.
[38]. Qi K, Cheng B, Yu J, Ho W (2017) Review on the improvement of the photocatalytic and antibacterial activities of ZnO. J Alloys Compd, 727:792-820.
[39]. Liang Y, Demi, H, Wu Y, Aygun A, Tir, RNE, Gur T, Vasseghian, Y. (2022) Facile synthesis of biogenic palladium nanoparticles using biomass strategy and application as photocatalyst degradation for textile dye pollutants and their in-vitro antimicrobial activity. Chemosphere, 306:135518.
[40]. Syed A, Elgorban AM, Bahkali AH, Zaghloul NS (2021) Coupling of nano-spinel MgFe2O4 on Co3O4 for heterogeneous photocatalysis and antibacterial applications: Insights of optoelectrical properties. Colloid Interfac Sci, 44:100467.
[41]. Grabowska E. (2016) Selected perovskite oxides: Characterization, preparation and photocatalytic properties—A review. Applied Catalysis B: Environmental, 186:97-126.
[42]. Ahmad T, Farooq U, Phul R (2018) Fabrication and photocatalytic applications of perovskite materials with special emphasis on alkali-metal-based niobates and tantalates. Ind. Eng Chem Res 57(1):18-41.
[43]. Zhou X, Chen Y, Mei H, Hu Z, Fan Y (2008) A facile route for the preparation of morphology-controlled NaTaO3 films. Appl. Surf. Sci, 255(5):2803-2807.
[44]. Wang C, Yin R, Yin H, Kang H, Yuan X, Yue Z, Ren H (2024) Reduced Ag NPs-modified NaTaO3 layer improves photocatalytic degradation and antimicrobial ability through LSPR effect and doping behavior. Appl. Surf. Sci, 678:161079.
[45]. Pallavi KM, Mamatha GP, Nagaraju G, Soundarya TL (2023) Facile synthesis of NaTaO3 nanoparticles and fabrication of nanostructured NaTaO3 for detection of dopamine. Inorg Chem Commun, 158:111427.
[46]. Chen, Q., Yao, Y., Li, X., Lu, J., Zhou, J., & Huang, Z. (2018). Comparison of heavy metal removals from aqueous solutions by chemical precipitation and characteristics of precipitates. Journal of , 26, 289-300.
[47]. Swathi S, Yuvakkumar R, Ravi G, Kumar P, Hong SI, Nasif O, Velauthapillai, D (2021) Orthorhombic tantalum pentoxide nanorods for electrochemical applications. Ceramics International, 47(11):15253-15259.
[48]. Alhaddad M, Ismail, AA (2020) Comparative study on mesoporous M/LaNaTaO3-based photocatalysts (M= Ag, In, and Nd) for hydrogen generationJ. Taiwan Inst Chem Eng, 117:144-155.

[49]. Zak AK, Majid WA, Abrishami ME, Yousef, R (2011) X-ray analysis of ZnO nanoparticles by Williamson–Hall and size–strain plot methods. Solid State Sci, 13(1):251-256.
[50]. Dang TT, Nguyen TLA, Ansari KB, Nguyen VH, Binh NT, Phan TTN, Trinh QT (2021) Perovskite materials as photocatalysts: Current status and future perspectives. Nanostructured Photocatalysts, 169-216.
[51]. Arandiyan H, Mofarah SS, Sorrell CC, Doustkhah E, Sajjadi B, Hao D, Maschmeyer T (2021) Defect engineering of oxide perovskites for catalysis and energy storage: synthesis of chemistry and materials science. Chem Soc Rev, 50(18):10116-10211.
[52]. Li X, Zang J, (2009) Facile hydrothermal synthesis of sodium tantalate (NaTaO3) nanocubes and high photocatalytic properties, J Phys Chem C 113:19411–19418